Waste and Biomass Valorization (2021) 12:5743–5761
https://doi.org/10.1007/s12649-021-01394-1

ORIGINAL PAPER

Valorization of Jute Biomass: Performance of Fiber–Cement Composites Extruded with Hybrid Reinforcement (Fibers and Nanofibrils)

Camila Soares Fonseca[1] · Mário Vanoli Scatolino[2] · Luiz Eduardo Silva[2] · Maria Alice Martins[3] · Mário Guimarães Júnior[4] · Gustavo Henrique Denzin Tonoli[2]

Received: 11 June 2020 / Accepted: 10 February 2021 / Published online: 23 February 2021

Abstract

In this study, the characteristics of jute fibers and cellulose nanofibrils (CNFs) and their impacts on mechanical strength were compared, particularly from the standpoint of their application as reinforcement in extruded fiber–cement composites. Raw jute fibers were subjected to an alkaline treatment before being fibrillated into CNFs. The fiber–cement composites were produced with jute fibers (0.5% and 2%) and CNFs (0.5% and 2%) via extrusion process. Both percentages of reinforcement were based on the cement mass. In addition, hybrid composites with a mixture of fibers and CNFs were produced. Hydroxypropyl methylcellulose and carboxylic polyether were used as additives to improve the mixture's rheology. The composites were subjected to natural weathering for 5 months before being analyzed for their physical and mechanical properties. CNFs and jute fibers subjected to NaOH treatment presented a higher initial degradation temperature (T_{onset}). The apparent porosity decreased for all compositions studied, reaching a 75% reduction for the sample reinforced with 2% CNFs. Fiber–cement with a hybrid reinforcement of 1.5% CNFs + 0.5% fibers exhibited the strongest mechanical performance. All compositions showed a decrease in the modulus of elasticity after natural weathering. In contrast, the modulus of rupture and the limit of proportionality showed an average gain of 1 MPa for fiber–cement composites produced with hybrid reinforcements. The better mechanical performance of the hybrid formulations may be owing to the synergistic work of the fibers and CNFs, suggesting the potential of cellulose CNFs for use as reinforcement in cement-based composites.

✉ Mário Vanoli Scatolino
mario_paraiso@hotmail.com; marioufla@estudante.ufla.br

Camila Soares Fonseca
camilasfonseca8@hotmail.com

Luiz Eduardo Silva
lesilvaflorestal@gmail.com

Maria Alice Martins
maria-alice.martins@embrapa.br

Mário Guimarães Júnior
mgjunior@cefetmg.br

Gustavo Henrique Denzin Tonoli
gustavotonoli@ufla.br

[1] Department of Engineering, Federal University of Lavras, Lavras, MG, Brazil

[2] Department of Forestry Science, Federal University of Lavras, Lavras, MG, Brazil

[3] Embrapa Instrumentação, São Carlos, SP, Brazil

[4] Department of Eletromechanical, Federal Center for Technological Education of Minas Gerais, Araxa, MG, Brazil

Graphic Abstract

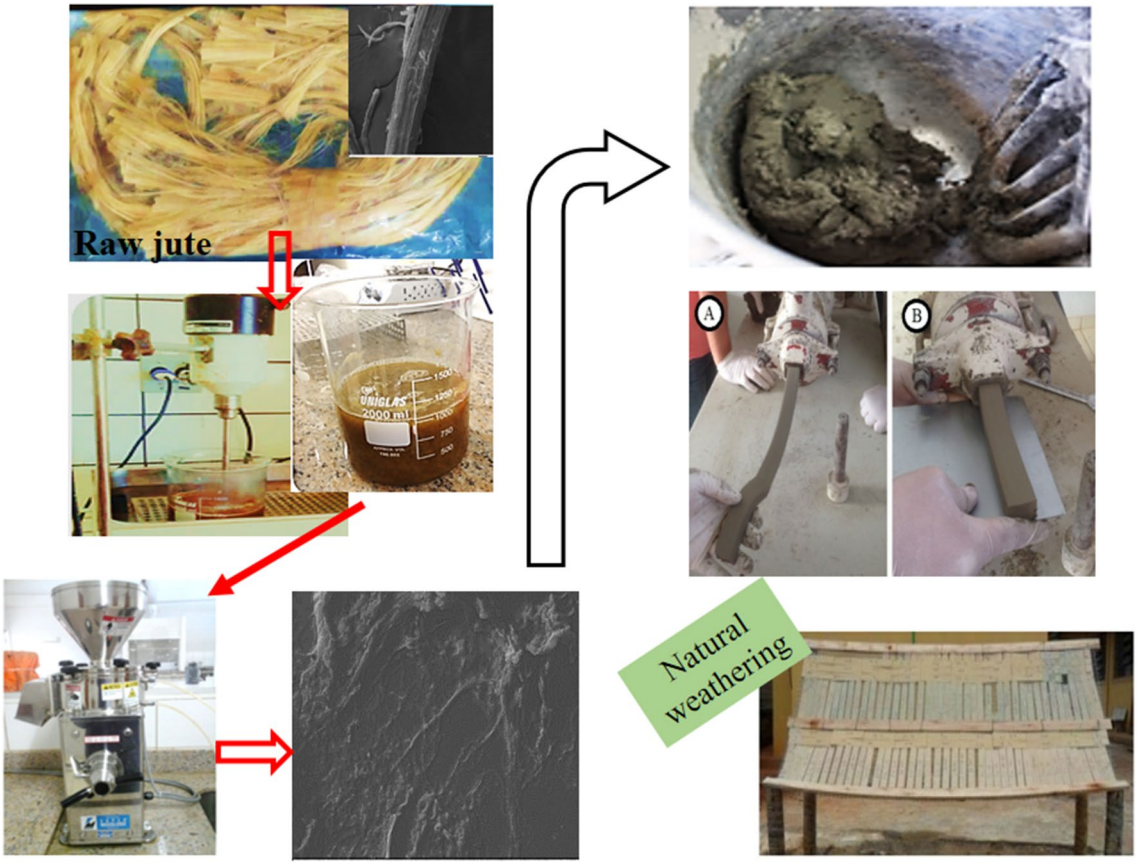

Keywords Mechanical fibrillation · CNF · Cellulose fibers · Lignocellulose fiber

Statement of Novelty

Studies that characterize composites reinforced with CNFs which present networks that can provide excellent mechanical properties to fiber–cement, especially after weathering, remain scarce. This work reports on a study that investigated how natural weathering, including exposure to rain, wind, humidity, and sunlight, can influence the mechanical properties of fiber–cement composites. The results obtained may contribute to the production of natural weathering-resistant fiber–cement composites using natural and renewable materials, which are widely available and at low cost.

Introduction

Jute plants (*Corchorus* sp.) are an attractive source of fibers because they are easily obtained, highly available, and inexpensive [1]. Originally from India, the jute plant is a resilient vegetable fiber source widely cultivated in some regions of Asia, such as China, India, and Bangladesh. Additionally, it is one of the most important temporary crops produced in Brazil, mainly in the states of Amazonas and Bahia [2].

In Brazil, jute cultivation has become one of the main economic activities for the Amazon population. Jute can be cultivated in river gutters without causing deforestation or water degradation. The planting cycle takes 6 months and coincides with the flood and ebb periods of the rivers. Owing to their high mechanical strength [3], these fibers are used to produce fabrics, packaging, belts, and twine, in addition to rugs and carpets. The strong mechanical properties of this fiber also enable its use in polymer composites, which has been widely studied by several research groups [4]. The use of jute in composite materials has been increasingly gaining popularity in recent years, such as its use in composites associated with glass fibers [5], reinforcement in polymeric composites [6, 7], cementitious matrices [8, 9], and new advances in nanotechnology that enable the use of jute fibers in the development of new

materials [10, 11]. Because jute fibers are rich in cellulose (45–72%) [12], they can be used as feedstock for the production of CNFs. These structures are produced from the fibers after being subjected to chemical, enzymatic, or mechanical treatments, with final diameters measuring less than 100 nm [11]. CNFs are formed by a linear association of cellulose chains that form both amorphous and crystalline regions and may form entangled networks with a high surface area.

The preparation of CNFs from cellulose fibers includes several methods that can be used in combination or independently, such as refining [13], cryocrushing [14], microfluidization [15], milling [16], steam explosion [17], TEMPO oxidation [18], and mechanical fibrillation [19, 20]. Mechanical fibrillation allows for the delamination of the fiber cell wall by multiple shearing cycles. The high shear is caused by the action of two closely placed circular stones inside the grinder, one being stationary and the other rotating at a high frequency. Mechanical methods can be carried out with a lower reagent content than that in the case of chemical hydrolysis to obtain cellulose nanocrystals/nanowhiskers [21]. CNF production can be facilitated by pretreatments, which increase the yield and reduce energy consumption during fibrillation. Alkaline pretreatment has been reported in the literature for the removal of non-cellulosic components, such as extractives, hemicelluloses, and lignin [22–25]. It has also been shown to be effective in facilitating fibrillation.

In cementitious matrices, including fibers, their microstructure is reinforced, which increases the impact strength of the fragile matrix and minimizes matrix cracking [26]. Vegetal fibers associated with cement composites have been employed because of their low cost, availability from renewable sources, lack of environmental toxicity, and excellent mechanical properties [27–33]. Many vegetal fibers or CNFs originating from them, such as jute [1], eucalyptus [26, 34], pine [35], corn cob [36], date palm [37], and bamboo [38], have the potential to be used as reinforcements in fiber–cement composites. The high nanoscale interaction between elements may form a percolated network connected by hydrogen bonds, which allows for the effective dispersion of CNFs in the matrix [39]. CNFs could be more effective as composite reinforcements when compared to their equivalent macro/microscale because of their greater specific area available for connection with the matrix. However, comparing the reinforcement with fibers and CNFs in the fiber–cement and their impact on the composite microstructure and mechanical performance still requires further investigation. In this study, the influence of jute fibers and CNFs as reinforcements in extruded fiber–cement composites and the impact on their mechanical strength after 28 days of curing and natural weathering are analyzed.

Materials and Methods

Obtainment and Pretreatment of the Jute Fibers

Jute fibers (*Corchorus* sp.*)* were provided by Brasjuta da Amazônia S.A. The fibers were cut about 10 mm in length, and ground in a knife mill (Marconi, SP—Brazil) equipped with a 10-mesh sieve (2.0 mm). The fibers were alkaline pretreated according to the methods described in Yue et al. [40]. For each 5 g of fiber, 100 mL of 5% (m/v) NaOH solution was used. The pretreatment was performed at 80 °C under constant stirring at 1500 rpm for 2 h. Posteriorly, the fibers were rinsed to remove NaOH excess and oven-dried at 40 °C for 24 h.

Chemical Analysis of the Jute Fibers

The total extractives content was determined as established in NBR 14,853 standard [41] using toluol–ethanol extraction followed by washing with hot-water. The insoluble lignin content was measured by acid hydrolysis with sulfuric acid (72% v/v) followed by boiling in hot-water, according to the NBR 7989 standard [42]. The holocellulose content (cellulose + hemicelluloses) was obtained according to the methodology proposed by Browning [43]. Afterwards, the cellulose content was determined by reacting holocellulose with potassium hydroxide, following the methodology proposed by Kennedy et al. [44]. The hemicelluloses content was calculated by subtracting the cellulose content from the holocellulose content. A furnace at 525 °C was used to assess the ash content, according to the NBR 13999 [45].

Production of the Jute CNFs

Alkali-treated jute fibers (1% m/v) were soaked in water at room temperature (± 21 °C) for 48 h and then stirred at 2000 rpm for 1 h. The treated fibers were processed in a Massuko-Sangyo® SuperMasscolloider grinder (MKCA6-2) at 1500 rpm, with a 0.01 mm gap between the silicon-carbide stone discs. The CNFs were obtained after 30 passages through the grinder based on methods suggested in previous studies [19, 20, 37].

Microstructure of the Fibers/CNFs

A scanning electron microscope (Zeiss DMS 940A), operating at 15 kV, with tungsten filament, was used to obtain micrographs of the fibers and CNFs. The samples were spread over double-sided carbon adhesive strips, previously fixed over aluminum sample holders (*stubs*), and gold-coated before visualization. The CNFs were additionally visualized

by a transmission electron microscope (FEI Tecnai 12) operating at 120 kV. CNFs suspensions were stained with uranyl acetate and a drop was deposited on formvar/carbon-coated with 400-mesh (0.037 mm) copper grids and dried before the analysis. The average diameter of the CNFs was measured using the analyzer software *ImageJ*. Approximately 500 measurements were taken to evaluate the diameter distribution of the CNFs filaments.

Thermogravimetric Analysis (TGA) of the Fibers/CNFs

The thermal analysis of raw jute, NaOH-treated and CNFs was conducted in a TA Instruments thermal analyzer TGA Q500, with a heating rate of 10 °C/min. The analysis was performed under two conditions to understand the fibers and CNFs behavior during both pyrolysis and combustion. The pyrolysis occurs under inert atmosphere (N_2; gas flow 50 mL/min), and is defined as the thermochemical degradation of a substance or material, when heat is applied in total absence of an oxidant [46]. The combustion occurs under oxidative atmosphere with synthetic air, (80% N_2 and 20% of O_2), with gas flow of 100 mL/min. The temperature in which degradation begins (T_{onset}) was established according to Scatolino et al. [47], by the intersection of the extrapolation line of the linear region of the curve (with no mass loss) with the tangent curve of the first stage of thermal degradation. The curves of derivative thermogravimetric analysis (DTG) were drawn to facilitate the visualization of degradation peaks. The percentage of volatile matter was determined by the difference between the total mass of the sample and the percentage of mass lost in the first linear region of the curve. The amount of mineral residues was represented by the mass remaining after the end of the analysis.

X-ray Diffraction of the Fibers/CNFs

Typical X-ray diffractograms of the starting jute, NaOH-treated, and CNFs were obtained by a Rigaku diffractometer XRD 600, operating at 30 kV, 30 mA and radiation of CuKα = 1.54056 Å. The scanning was performed at a 2θ/min rate from 5° to 40° (2θ). According to previous works [48–51], Segal index is not suitable to estimate the cellulose crystallinity because of many features regarding its crystal configuration, such as crystal size and degree of polymorphism. Then, the crystallinity was calculated by the amorphous and crystalline fractions (Eq. 1).

$$C_f = \frac{C_a}{C_a + A_a} \tag{1}$$

where C_f is the crystalline fraction; C_a is the sum of the areas under the theoretical crystalline curves and A_a is the sum of the areas under the theoretical amorphous curves. The program Mercury 3.7 was used to produce theoretical diffraction patterns for crystalline and amorphous fractions, varying the peak width at half maximum (PWHM) of cellulose Iβ and cellulose II, respectively [50]. For the amorphous halo, it was used cellulose II CIF (Crystallographic Information File) with PWHM of 9 and a correction factor [52]. Cellulose Iβ has been chosen for the calculations because it is the most abundant cellulose polymorph for higher plants in nature [40]. All measurements were carried out on the theoretical curves after the fitting process. The CIF files were obtained from complementary data in French [48] and edited to fit the theoretical curve into the experimental one according to Correia et al. [49].

Crystallite size was determined by Scherrer's equation (Eq. 2) described by Langford and Wilson [51]. Additionally, the number of cellulose chains in the crystals was determined according to Ballesteros et al. [52].

$$D = \frac{k\lambda}{\beta \cos\theta} \tag{2}$$

where D is the perpendicular size to the lattice plane (200); k is the correction factor (0.9); λ is the X-ray radiation wavelength (1.54 Å); β is the PWHM of the diffraction peak (in radians) and θ is the diffraction angle of the peak (22.7°).

Fourier-Transform Infrared Spectroscopy (FTIR) of the Fibers/CNFs

The samples of starting jute, NaOH-treated, and CNFs were crushed and homogenized before the analysis. A Shimadzu spectrometer IRAffinity-1 was used to obtain the spectra, using 32 scans, ranging from 400 to 4000/cm and resolution of 2/cm. Posteriorly, the samples were dried at 40 °C until constant mass and then incorporated to KBr in a proportion of 1:100 (m:m).

Production of the Fiber–Cement Composites

The cementitious matrix was composed of Ordinary Portland Cement CP V-ARI, corresponding to Type I (ASTM-C150) and ground agricultural limestone. Hydroxypropyl methylcellulose (HPMC) and carboxylic polyether (ADVA) were applied as additives to improve the mixture's rheology. For all formulations (Table 1), 1% (based on the cement mass) of both additives was used, as described by Teixeira et al. [53].

Cement, limestone and reinforcement (jute fibers or CNFs) were first mixed in a beater for approximately 5 min to efficiently disperse the reinforcement. Afterwards, the water and additives were added (Fig. 1). The whole

Table 1 Compositions of the extruded composites

	Reinforcement	Water/cement	Cement	Limestone
			Based on cement mass (%)	
Control	Unreinforced	0.30	68.0	30.0
0.5F	0.5% fibers	0.34	67.5	30.0
2.0F	2.0% fibers	0.33	66.0	30.0
0.5 N	0.5% CNFs	0.41	67.5	30.0
2.0 N	2.0% CNFs	0.42	66.0	30.0
F0.5 + N1.5	0.5% fibers + 1.5% CNFs	0.41	66.0	30.0
F1.0 + N1.0	1.0% fibers + 1.0% CNFs	0.39	66.0	30.0
F1.5 + N0.5	1.5% fibers + 0.5% CNFs	0.39	66.0	30.0

The 2% remaining in the composition refers to HPMC and ADVA additives

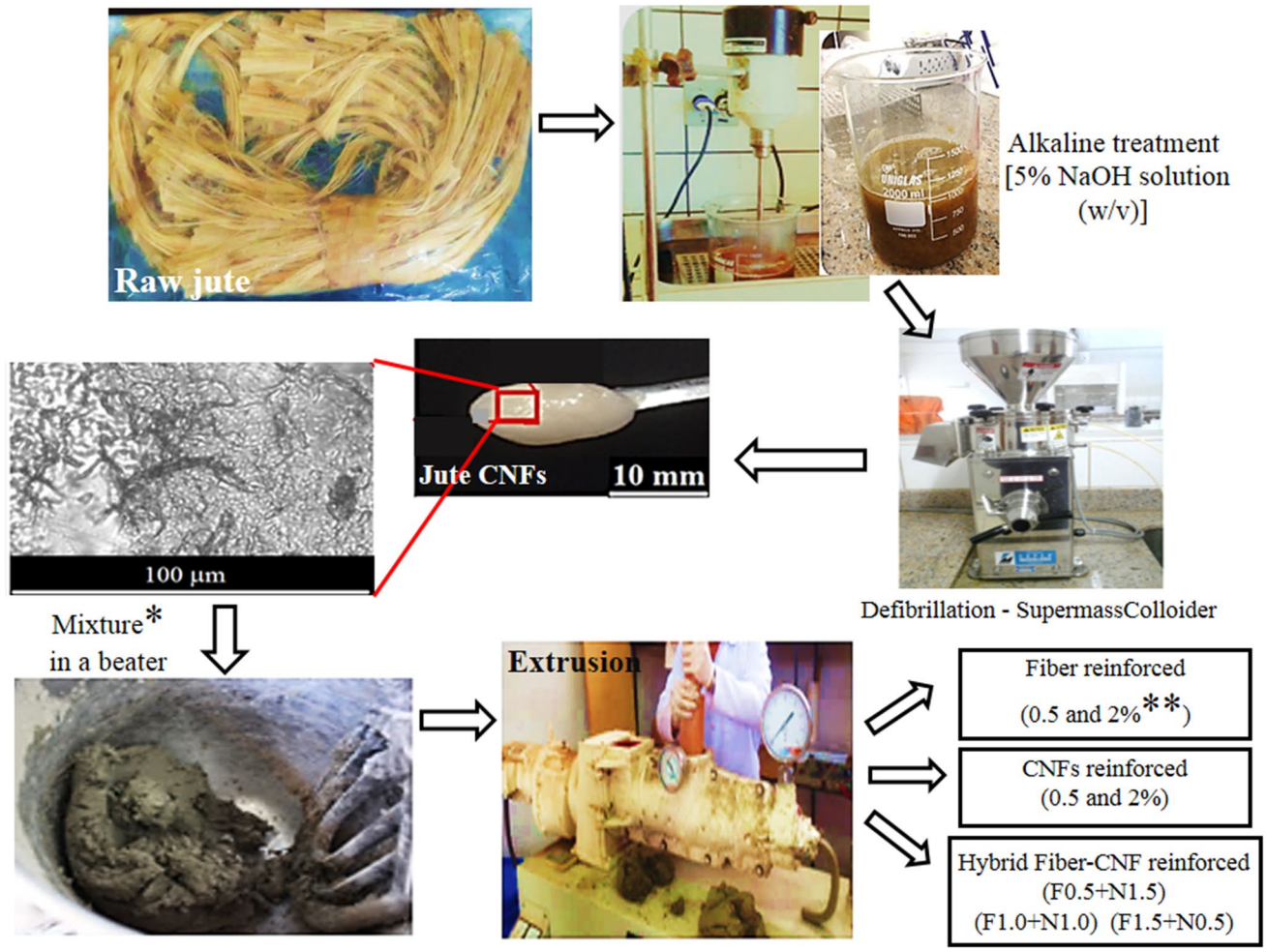

Fig. 1 Scheme of the composites production. *Fibers and/or CNFs + Water + Cement + Limestone + HPMC + ADVA; **Based on cement mass

formulation was then mixed for approximately 10 min for homogenization.

In mixtures with 2% of jute fibers (2.0F), there was some loss of its pseudoplastic behavior in the beginning of the extrusion process. This can be related to a high volume of fibers (2% in relation to cement mass) were used as reinforcement, resulting in their interlacing and clogging of the extruder die. This mixture behavior was not observed when 2% (by mass) of CNFs (2.0 N) were used as reinforcement, which may be explained by the higher water/cement ratio (0.42) of this formulation. The water/cement ratio was higher when CNFs were used as reinforcement

when compared to formulations with natural jute fibers. After CNFs production, the excess water from the gelatinous suspension was removed, but a considerable amount of water remained in the suspension (90% of moisture). This residual water increased the water/cement ratio. The composites were obtained with nominal dimensions 200 × 30 × 20 mm in a Verdés single-screw extruder. After molding, the composites were stored in a sealed container, with saturated humidity, at room temperature (± 21 °C) for 28 days.

Apparent Density and Apparent Porosity of the Composites

Physical properties such as apparent density and apparent porosity were analyzed according to ASTM C 948-81 standard [54]. The samples were immersed in water at room temperature (± 21 °C) for 24 h to assess wet mass (water-saturated composite with removal of the excess water from the surface) and immersed mass. Posteriorly, the samples were oven-dried at 80 °C for 24 h to determine the dry mass. Six samples were evaluated for each formulation. Equations (3) and (4) were used to assess the physical properties.

$$Apparent\ density = \frac{Dm}{Im - Wm} \times \rho \tag{3}$$

$$Apparent\ porosity = \frac{Wm - Dm}{Im - Wm} \times 100 \tag{4}$$

where Dm is the dry mass (g); Wm is the water-saturated mass (g) from the composite with removal of the excess water from the surface; Im is the mass (g) after water immersion (24 h) and ρ is the density (g/cm^3) of the liquid where the samples were immersed (distilled water; $\rho = 1$ g/cm^3).

Mechanical Properties of the Composites

The mechanical tests were performed using a universal testing machine TIME-SHIJIN WDW-20E (load cell 20 kN). A configuration with three points (lower gap 150 mm) was used to determine the modulus of rupture (MOR), limit of proportionality (LOP), modulus of elasticity (MOE) and tenacity in static bending. The configuration and calculations followed the procedures suggested in Rilem [55] and described in detail in previous studies [56, 57]. For each formulation, six samples of fiber–cement were evaluated.

Natural Weathering of the Composites

The samples were weather-exposed, in a bench with an inclination of 45° with the surface of the terrain, facing the "true north" for 5 months, from February to June, which correspond to the end of the summer and beginning of winter in the Southern Hemisphere. The bench was located in the city of Lavras, State of Minas Gerais, Brazil, where the mean annual temperature is 27 °C, relative humidity is around 60%, 919 m of altitude, 21°14′43″ S of latitude and 44°59′59″ W of longitude. During this period, the maximum and minimum temperatures were 33 and 15 °C, the average wind speed was between 5.2 and 14.8 km/h, the rainfall was approximately 1300 mm/year and the average relative humidity was around 63%. During the 5 months abovementioned, there was an intense variation in weather conditions in the region. The samples were exposed to high and low temperatures, rainy and dry climates, with few or much wind, among other weather conditions. These factors, among others, may influence the mechanical and microstructural properties of the fiber–cement composites.

Microstructure of the Composites

The evaluation of the cementitious composites microstructure was performed through scanning electron microscopy (SEM) by a JMS 6510 (JEOL®) microscope operating at 10 kV. The samples were placed on double-sided carbon adhesive strips, previously fixed over aluminum sample holders (stubs) and gold-coated before the visualization. The analysis was performed on the fracture surface of the composite samples after the rupture caused by the mechanical tests.

Results and Discussion

Characterization of the Fibers/CNFs

Chemical Analysis of the Fibers/CNFs

NaOH-treated jute fibers showed higher cellulose content (Table 2). The cell wall structure of vegetal fibers is formed by cellulose micro/nanofibrils and consequently had a considerable influence on the physical and mechanical properties of the fibers [58].

Table 2 Average and standard deviation of the chemical components of raw jute fibers and after the pretreatment with NaOH

Chemical components	Jute fibers	
	Raw jute (%)	NaOH-treated (%)
Total extractives	1.9 ± 0.2[a]	-
Lignin	11.8 ± 1.2	11.7 ± 0.9
Cellulose	53.1 ± 3.1	75.0 ± 4.4
Hemicelluloses	32.3 ± 1.1	12.8 ± 1.3
Ashes	0.9 ± 0.1	0.4 ± 0.1

[a]Standard deviation

The degree of influence of hemicelluloses content on fiber fibrillation is controversial. During mechanical fibrillation, hemicelluloses content influences the efficiency of the process, whereas its reduction enables micro/nanofibrils to be individualized [23, 59]. However, previous studies have found that hemicelluloses may also act as an inhibitor of CNFs coalescence during filtration/draining of excess water, and it may contribute to the overall mechanical strength when used in composites [60, 61]. The higher the hemicellulose content, the higher the efficiency of the nanofibrillation process [62]. Scatolino et al. [47] noted that some remaining hemicelluloses did not prevent CNFs from being formed. Otherwise, the removal of hemicelluloses to levels of 9–12% may facilitate fiber deconstruction [63]. Lignin was responsible for the adhesion between the inner layers of the fiber cell wall [61]. The NaOH treatment performed did not change the lignin content of the treated fibers compared to the raw jute fibers.

Thermogravimetric Analysis (TGA) of the Fibers/CNFs

The initial mass loss (approximately 10% at 120 °C) for all samples corresponded to the volatilization of some residual moisture in the fiber. The main thermal degradation occurs between 250 and 350 °C (Fig. 2), which corresponds to the pyrolysis of the cellulose components [30]. Degradation by pyrolysis occurs slowly and is irreversible. The final residue is mainly composed of inorganic and unconverted organic materials.

After reaching the initial degradation temperature (T_{onset}), an irreversible degradation of the biomass begins. Therefore, the processing temperature of the composite should not exceed T_{onset}. This temperature must be considered as the maximum temperature for processing lignocellulosic materials [64]. Before raw jute fiber underwent pyrolysis, a high-intensity peak was observed in an inert atmosphere. The maximum decomposition temperature for the raw fiber was the highest when compared to that of the NaOH-treated fibers and CNFs. There was a reduction in

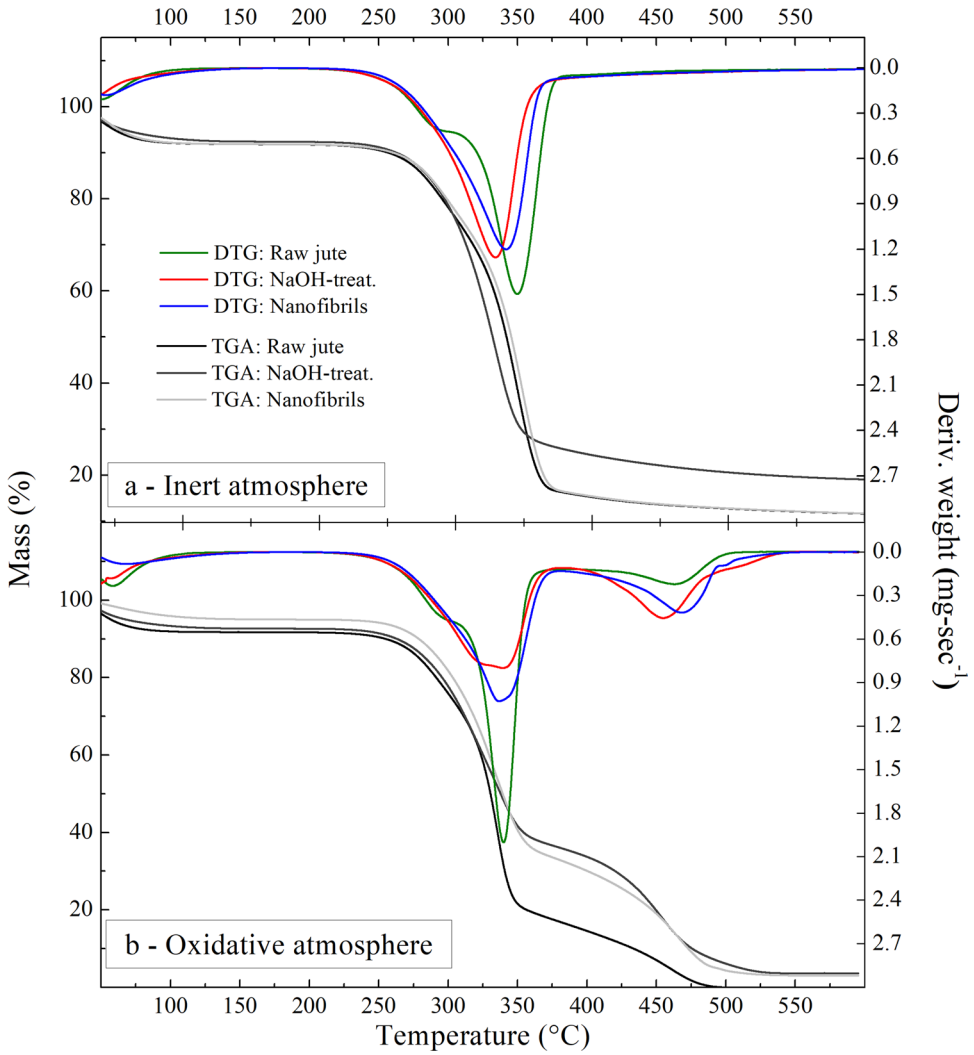

Fig. 2 Typical TGA and DTG curves of jute fibers and nanofibrils: **a** in inert atmosphere (100% N_2); and **b** in oxidative atmosphere (80% N_2 and 20% O_2)

Table 3 Thermal properties of the jute fibers and CNFs

Material	Atmosphere							
	T_{onset} (°C)		Degradation peak (°C)		Volatile matter (%)		Ash content (%)	
	Oxidative	Inert	Oxidative	Inert	Oxidative	Inert	Oxidative	Inert
Raw jute	278	299	338	355	8.1	7.8	0.5	11.6
NaOH- treated	281	299	337	345	7.3	7.5	3.5	18.4
CNFs	284	298	337	349	4.7	8.1	3.1	10.8

the maximum temperature of decomposition after treatment with NaOH, which slightly increased for the CNFs because of the realignment caused by the fibrillation process. In an oxidative atmosphere, NaOH-treated fibers and CNFs presented higher T_{onset} values when compared to raw fibers. This result was due to the lower relative hemicellulose content and higher relative cellulose content in NaOH-treated fibers and CNFs. Hemicelluloses begin their degradation process at lower temperatures than cellulose [47], so the decrease in hemicelluloses content increased the T_{onset} value of the NaOH-treated fibers and CNFs. In both atmospheres, the jute fiber took longer to move from the initial degradation (T_{onset}) to the peak of maximum degradation. This may have occurred because of the higher content of non-cellulosic components, such as extractives and hemicelluloses. Some kinds of extractives, mainly those soluble in acetone, may provide an increase in thermal stability and extend biomass combustion time [65]. During TGA in an oxidative atmosphere, two predominant peaks were observed. The first peak (275–375 °C) occurred because of the release of volatiles when the sample's chemical compounds were degraded during combustion, whereas the second peak (400–500 °C) indicated the carbonization of the formed charcoal [66]. CNFs shows a higher T_{onset} value (around 284 °C) than NaOH-treated fibers (around 281 °C) under an oxidative atmosphere (Table 3). Although these fibers have undergone high mechanical shear forces during fibrillation (which probably partially disrupted the crystal structures), they have been reorganized during oven drying when the samples were prepared for TGA [67].

The T_{onset} value practically did not change between jute fibers and CNFs during degradation in an inert atmosphere. Scatolino et al. [47] studied the thermal degradation in an oxidative atmosphere of Amazonian paricá fibers and CNFs and found T_{onset} values of 255 °C and 266 °C for NaOH-treated fibers and CNFs, respectively. The DTG curves presented a "shoulder" close to 300 °C for raw jute in both analyzed atmospheres. This specific region did not appear for NaOH-treated fibers and CNFs in the first degradation stage. This effect may be attributed to the removal of hemicelluloses. Additionally, with partial removal of non-cellulosic components in the raw fibers, the maximum rate of thermal degradation was intensified at approximately 340 °C.

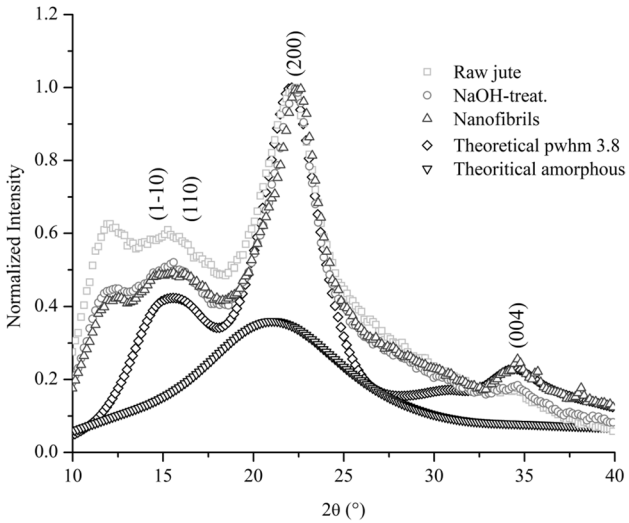

Fig. 3 Typical X-ray diffractograms of raw jute, NaOH-treated jute fibers (NaOH-treated) and jute nanofibrils

Table 4 Crystal structure of jute fibers and CNFs

Material	Crystalline fraction (%)	Crystallite size (nm)	Cellulose chains per crystallite
Raw jute	65	6.3	81
NaOH-treated	68	7.4	100
CNFs	66	7.3	100

X-ray Diffraction of the Fibers/CNFs

Both types of fibers and CNFs show a peak between 2θ values of 16.5° and 22.6°, representing cellulose I [68] (Fig. 3). NaOH pretreatment resulted in a reduction in hemicelluloses, which have an amorphous structure, increasing crystallinity (68%) comparable to the raw fiber (65%) (Table 4). This finding has also been reported in Correa et al. [69].

The raw fiber presented a broader peak at 22.3°, lattice plane (200), compared to NaOH-treated fibers, which

increased 4.6% in crystallinity and 17.5% in crystallite size. CNFs also showed an increase of 1.5% in crystallinity and 15.9% in crystallite size. Both increases were assumed to be due to the removal of the amorphous counterparts. The alkali-treated fibers exhibited peaks where 14.8° (1−10) and 16.2° (110) overlapped. The same behavior occurred in the theoretical curves when the PWHM was increased because of the amorphous contribution. Although the X-ray atterns of the CNFs were similar to those of the NaOH-treated jute fibers, the (1–10) and (110) peaks showed some degree of separation, whereas the peak at 34.6° (004) was more evident. The presence of the peaks listed above describes the typical pattern of cellulose Iβ [48]. The NaOH treatment used here was not sufficient to cause a change in the cellulose polymorphs, as observed when high alkali concentrations (e.g., higher than 12%) are used, transforming cellulose I into cellulose II [40].

Partial cellulose hydrolysis occurred during treatment, probably to non-crystalline instead of crystalline domains, because there was an increase in crystallinity values and crystallite sizes. The CNFs prepared from NaOH-treated fibers had a larger crystallite size. In some cases, the high shearing force of the mechanical process can damage the cellulose crystalline fraction. As previously discussed, drying may cause rearrangement of the amorphous parts of cellulose. Reorganization of the amorphous cellulose into crystals upon drying has also been reported [70, 71], where parallel glucan chains crystallized into cellulose I after drying. In addition, the increase in crystallite size from the raw fibers to the NaOH-treated ones resulted from more cellulose chains being packed into the crystallite (see Table 4). Tonoli et al. [67] found a decrease in crystallite size when comparing commercial eucalyptus pulp fibers and CNFs due to the high shear that occurred during mechanical fibrillation, which damaged the crystallites.

FTIR Analysis of the Fibers/CNFs

Raw fibers show a lower absorption intensity close to 3330/cm (Fig. 4), which corresponds to the OH stretching vibration [72] and provided considerable information concerning hydrogen bonding in jute fibers or CNFs. The higher intensity of OH vibration in the NaOH-treated fibers and CNFs is due to the higher cellulose content (see Table 2).

The peak observed at approximately 1740/cm in the raw fibers refers to the axial deformation of C=O, which is attributed to the ester-uronic and acetyl groups of hemicelluloses or the ester connections of the carboxylic group of lignin [73]. This peak disappeared after the NaOH treatment and the individualization of CNFs due to partial removal of hemicelluloses, again corroborating the results in Table 2.

Peaks between 1462 and 1598/cm refer to the axial deformation of C=C in the aromatic rings of lignin [47]. The peaks located in this range for the NaOH-treated fibers and CNFs were lower than those observed for the raw fiber. This result also agrees with the chemical analysis, which reported the presence of lignin after the NaOH treatment. The mechanical fibrillation used to produce CNFs did not change their chemical structure because it only severed hydrogen bonds through shearing forces, resulting in the

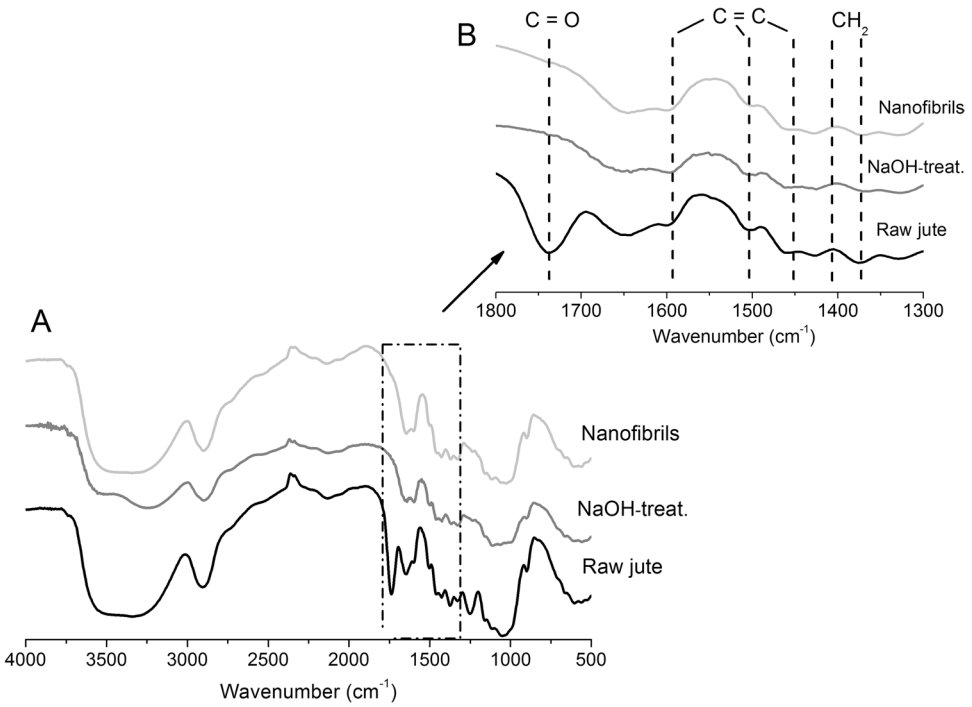

Fig. 4 FTIR spectra of raw jute, NaOH-treated jute fibers (NaOH-treat.) and jute nanofibrils; **a** showing the full spectra from 4000 to 500/cm; **b** detail of the region between 1800 and 1300/cm

individualization of the micro/nanofibril bundles from the cell wall.

Peaks between 1370 and 1430/cm, assigned to the symmetric CH_2 bending vibration of the cellulose crystalline domains, decrease with lower crystallinity [67]. The peaks located in this range for raw jute fibers, NaOH-treated fibers, and CNFs did not show significant differences, although the crystalline fraction of the raw fibers was lower than that of the NaOH-treated fibers and CNFs (see Table 4).

Morphological Analysis of the Fibers/CNFs

Mechanical fibrillation reduced the average diameter of the jute fibers, increasing their swelling capacity due to fracturing and detachment of the nanofibrils, as well as increasing the surface area when dispersed/individualized. In addition to the changes in chemical composition, NaOH treatment leads to irreversible changes in the fiber surface [47]. SEM images show that the surface of the NaOH-treated fibers is cleaner than that of the raw jute fibers (Fig. 5). However, some residues were still observed on the surface of the NaOH-treated fibers. Higher exposition of the cellulose fibrils was observed for the NaOH-treated fibers. With the dissolution of the external layers of the cell wall, cellulose micro/nanofibrils become more exposed, which facilitates their individualization [74]. CNFs are generated by fibrillation of the fiber cell wall and mainly consist of micro/nanofibril bundles with diameters between 10 and 40 nm [75–77].

As discussed previously, the shearing forces applied by the mechanical grinder were effective in deconstructing the fiber cell wall, producing CNFs dispersed in water [75]. The diameter distribution of the jute CNFs (Fig. 6) was obtained from measurements performed in transmission electron microscopy images and showed that approximately 80% of the filaments in the suspension had a diameter lower than 30 nm and an average diameter of approximately 31 nm. Lin et al. [78] studied CNFs produced from jute fibers and found diameters ranging from 5 to 20 nm, whereas Das et al. reported jute CNFs with an average diameter of 146 nm [79]. Lower diameters are expected to improve the performance of the composites because of the consequent higher aspect ratios of the filaments, which may improve percolation into the microstructure of the composite.

Properties of the Fiber–Cement Composites

The apparent density values of the fiber–cement composites tend to increase with the insertion of CNFs (Table 5). This

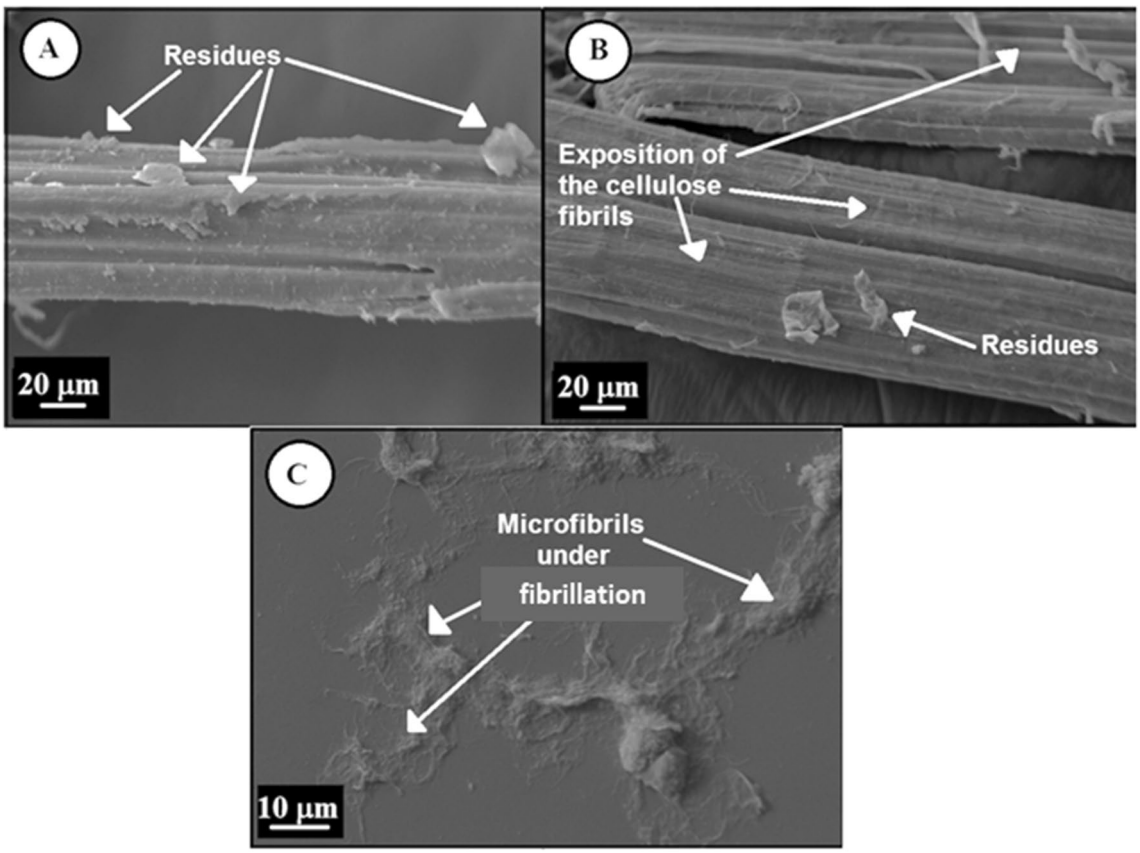

Fig. 5 Typical SEM images: **a** raw jute fiber; **b** NaOH-treated jute and **c** jute CNFs

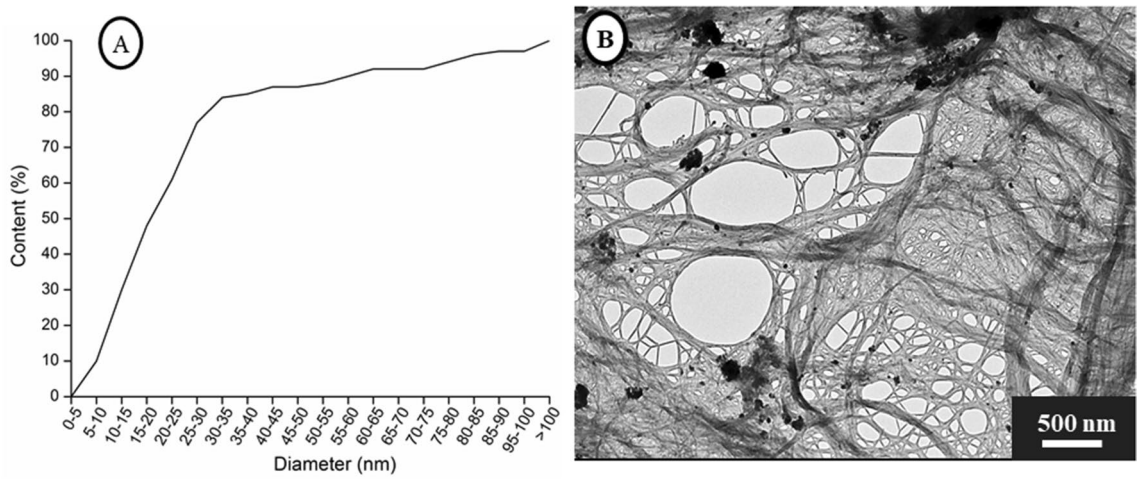

Fig. 6 Typical images of transmission electron microscopy; **a** histogram of the cumulative distribution of CNFs diameters, and **b** CNFs obtained by mechanical fibrillation

Table 5 Apparent density of the fiber–cement composites produced

Condition	Apparent density (g/cm^3)	
	28 days of curing	Natural weathering
Control	1.85 ± 0.02*b	2.00 ± 0.03c
0.5F	1.87 ± 0.01a	2.00 ± 0.04c
2.0F	1.82 ± 0.05c	2.02 ± 0.04c
0.5 N	1.88 ± 0.03a	1.96 ± 0.05d
2.0 N	1.88 ± 0.01a	2.28 ± 0.03a
F0.5 + N1.5	1.87 ± 0.01a	2.11 ± 0.04b
F1.0 + N1.0	1.84 ± 0.04b	2.07 ± 0.05b
F1.5 + N0.5	1.85 ± 0.03b	2.08 ± 0.04b

*Standard deviation; means followed by the same letter do not differ statistically by the Scott-Knott test at 5% of significance

may be due to the filling of cracks in the initial phases of cement hydration products. These products can deposit or reprecipitate mainly at the reinforcement–matrix interface [80]. Composites reinforced exclusively with CNFs (both 0.5% and 2%), the hybrid F0.5 + N1.5, and 0.5F did not differ statistically and presented the highest apparent density values. These results may be due to the optimization of raw material packaging during extrusion. In addition, CNFs act as plasticizers, improving the cohesion of the fiber–cement mixture [26].

The higher apparent density may be due to more compact matrices with fewer defects. In addition, the greater surface area of the CNFs provides better CNF–matrix interaction and, consequently, greater density. Because of the hydrophilic character of CNFs and the interaction of their hydroxyl groups with products from the cement hydration, it can be said that CNFs and other cellulose materials are compatible with cement products. Cement hydration tends to reduce the empty spaces around the reinforcement, consequently reducing the apparent porosity. The apparent density was higher for all formulations after natural weathering, probably because of the increased adhesion between the fibers and the cementitious matrix. Numerous "needles" were observed around the CNFs after 28 days of curing. These structures are probably monosulfoaluminates or ettringites [$(CA_6(Al(OH)_6)_2(SO_4)_3(H_2O)_{25,7})$] (Fig. 7), which provide greater porosity to the composite. After the composites were submitted to natural weathering, a significant reduction in ettringite "needles" was observed, which may be due to the reprecipitation of the hydration products of the cement inside or around the fibers and the natural carbonation that occurs throughout aging [81, 82]. This could increase the adhesion between fibers and matrices, resulting in a more compact structure and thus resulting in greater density and decreased porosity for the composites. The reduction in hydrated phases is the result of the natural carbonation that occurs during the aging of cementitious composites [56]. A large amount of ettringite around the fibers was found by Tonoli et al. [82] during an evaluation of the performance of extruded fiber–cement composite produced with cellulosic pulps modified with cellulose silanes after 28 days of curing.

Filling empty spaces or pores with cement hydration products increases apparent density [83]. The hybrid F0.5 + N1.5 displayed high apparent density values, probably because of the reinforcement provided by the fraction of CNFs, which in this case, resulted in synergy with the jute fiber. Among the composites reinforced with fibers, the 0.5F formulation stood out in density, probably because of the high degree of fiber mineralization combined with the higher water/cement ratio, which was responsible for the generation of higher quantities of hydrated products from cement. Regarding the hybrid cement composites, there was

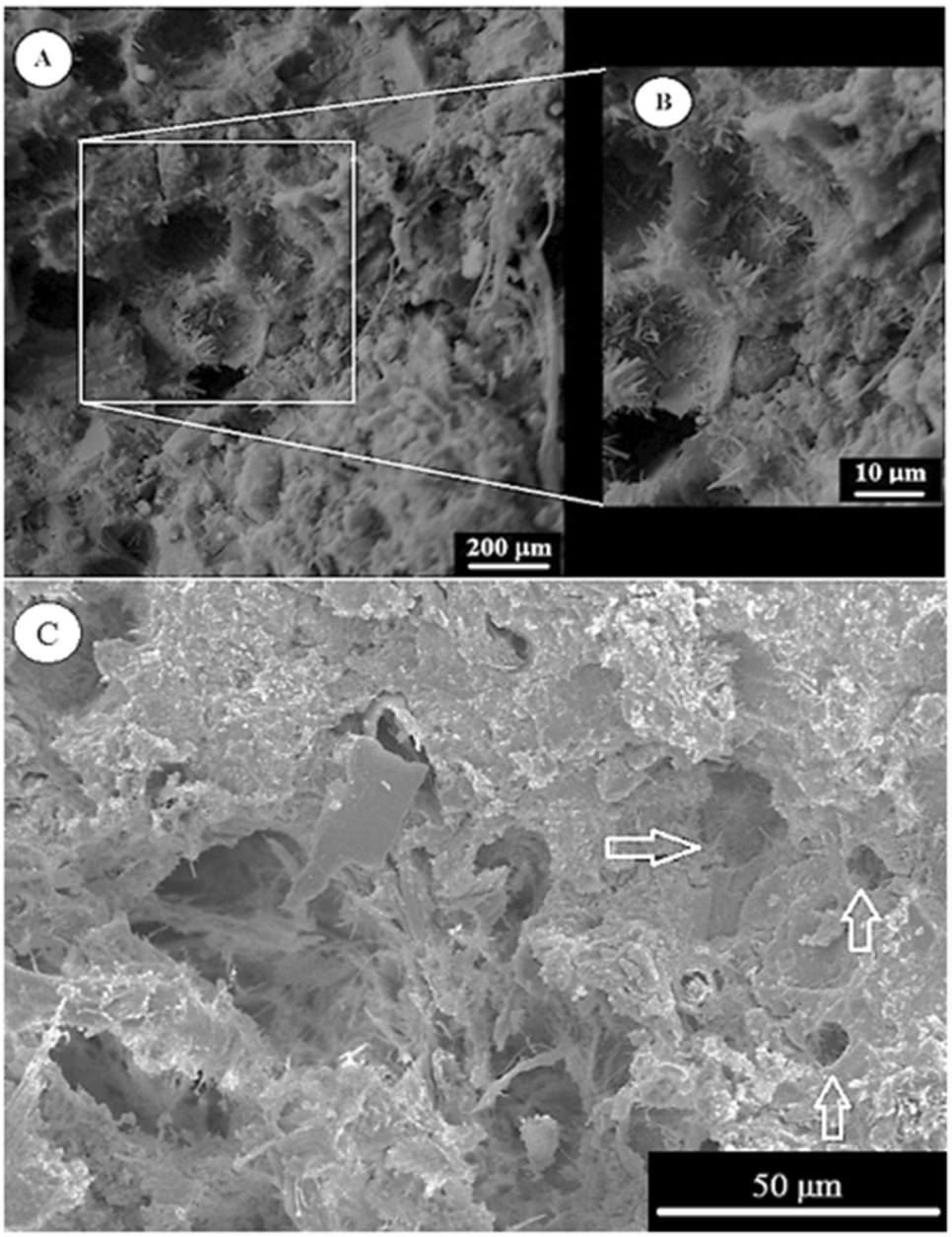

Fig. 7 Typical SEM of the fracture surface showing the presence of ettringite in the cementitious composites (2% of CNFs): **a** and **b** after 28 days of curing; **c** after natural weathering

a tendency for apparent porosity to increase with decreasing CNF percentage (Fig. 8).

The CNF size enables it to enter the meso and macropores of the cement. The mesopores are the interlaying spaces in the calcium silicate hydrate, with diameter sizes between 2 and 100 nm [84]. Macropores are capillary pores with sizes between 100 and 7000 nm [85]. The decrease of CNFs in the composites occurred simultaneously with the increase in the content of jute fibers, which may have contributed to the small increase in apparent porosity. Non-wood fibers are lighter than wood fibers [86]. The higher fiber content in the composite increases the probability of void formation [87]. Conversely, composites reinforced with 2% CNFs displayed higher apparent porosity in comparison to the control and the other formulations. This result may be due to the higher water/cement ratio of the composites reinforced with CNFs compared to other formulations. A high water/cement ratio results in the volatilization of free water, causing high porosity in the composite. Additionally, high porosity can lead to the presence of carbon dioxide in the paste [88]. In general, it is expected that a low water/cement ratio will elicit a low permeability effect in the cement paste [89].

Fiber-reinforced composites showed a reduction in apparent porosity values with an increase in the proportion of fibers and CNFs from 0.5 to 2% after natural weathering. As previously discussed, this reduction of approximately 28% is

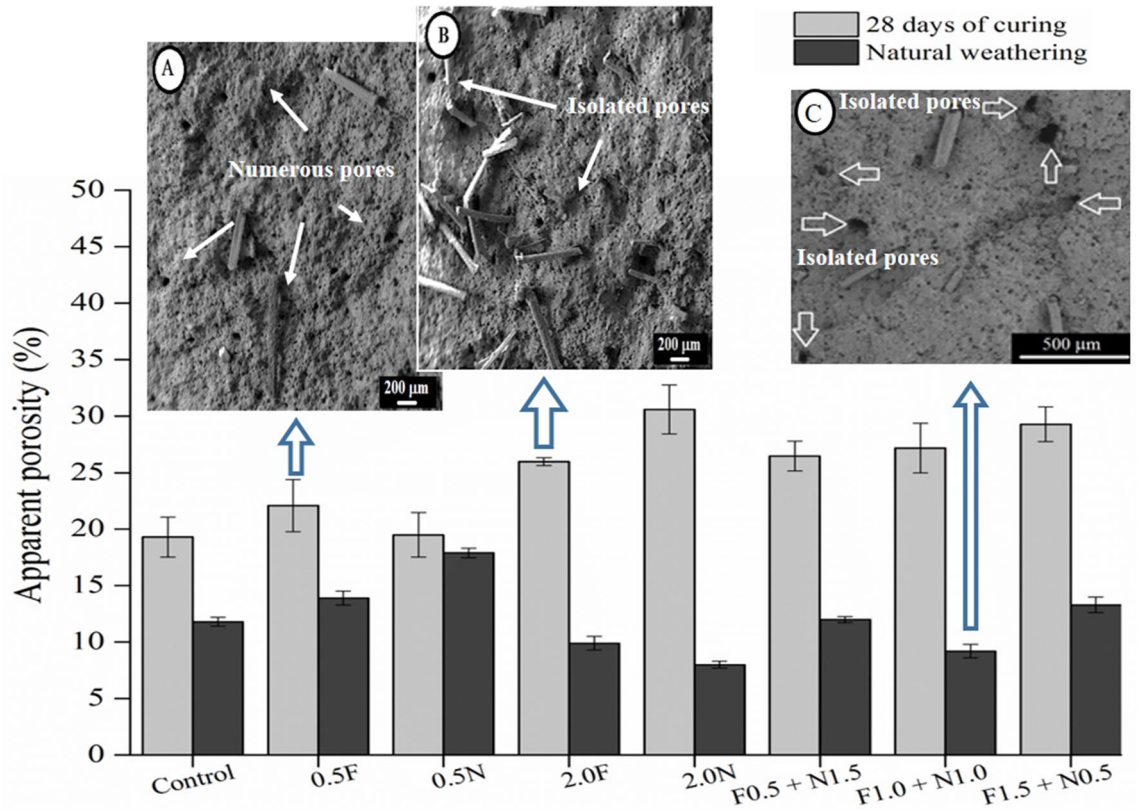

Fig. 8 Apparent porosity of the fiber–cements produced; **a** typical image (SEM) of the fiber–cement sample reinforced with 0.5% of fibers; **b** typical image (SEM) of the fiber–cement sample reinforced with 2% of fibers; **c** typical image (SEM) of the fiber–cement sample reinforced with 1% of fibers + 1% of CNFs after natural weathering

attributed to the filling of matrix pores by the cement hydration products and calcium carbonate from natural carbonation during weathering. The cracking process is due to the porosity of the fiber–cement composites, which can significantly affect the mechanical strength and be directly related to the fiber–matrix adhesion. Fibers in cementitious composites act as a macroscale reinforcement, preventing fragile fracture after crack initiation, owing to the distribution of microcracks along the material. CNFs act as nanoscale reinforcements (Fig. 9), connecting different grains and particles

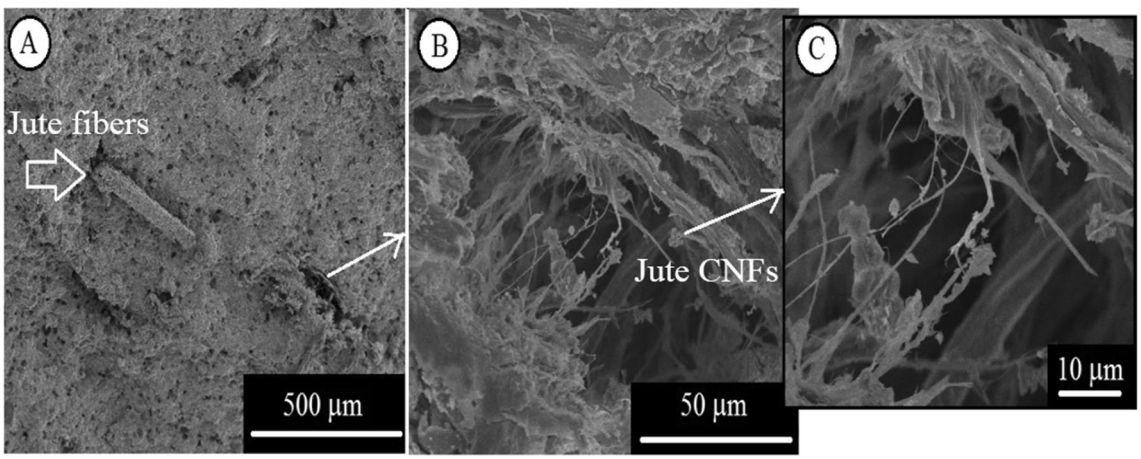

Fig. 9 Typical SEM images of: **a** fracture surface showing the adhesion between the fibers and the composites cementitious matrix with 0.5% of fibers and 1.5% of CNFs; **b** reinforcement acting on the microcracks; **c** zoom to the CNFs

of different sizes (mainly at the microscale) and forming a network of bonds that act as bridges for stress transfer. Consequently, the propagation of microcracks decreased in the cement matrix.

The MOE observed for all formulations is lower than that of the control (unreinforced) after 28 days of curing (Fig. 10), despite a slightly increasing trend for the 2.0F and F0.5 + N1.5 formulations. This result is due to the reduction in the fragile behavior of the composite by the insertion of fibers and CNFs as reinforcement. A lower MOE is expected because the fiber and CNF reinforcements ensure greater elastic deformation of the composite. Formulations with CNFs showed a predisposition to higher MOR than their equivalent with jute fibers, which was due to the greater surface area of the CNFs that strongly interacted with the cement matrix, even at small reinforcement levels. Similarly, the fiber–cement composites with higher CNF content, such as 2.0 N and the hybrid F0.5 + N1.5, exhibited higher MOR values.

Higher MOR values were attributed to the ability of CNFs to bond with the matrix. The MOR value indicates the stress distribution and the interaction between the fiber and matrix, in addition to the tensile strength. The larger surface area of the CNFs increased their interaction with the cement matrix because of the higher number of secondary bonds (mainly hydrogen bonds), resulting in a propensity for higher MOR values. In this context, because of the bonding of CNFs with the matrix, the nanofibrils could contribute to the increase in the tensile strength during the static bending of cementitious composites [90]. The increased dimensional variation of the jute fibers resulted in the fiber-matrix transitioning to the high-stress zone, leading to the collapse of the hydrogen bonds. The formulations reinforced with 2% of fibers and all formulations with CNFs showed increasing tendencies for both LOP and tenacity in relation to the control after 28 days of curing (Fig. 11).

The composites reinforced with 2% fibers displayed improved mechanical properties when compared to those reinforced with 0.5% fibers, especially for the values of MOR, LOP, and tenacity, which showed slightly greater behavior. Figure 8 shows the fracture aspect of both composites (2.0F and 0.5F), where it is possible to observe a structure with small and numerous micropores well-distributed throughout the composite reinforced with 0.5% fibers. Conversely, composites reinforced with 2% fibers had larger and more isolated pores. Composites reinforced with 2% CNFs and all hybrid formulations tended to have a greater LOP among the formulations studied after natural weathering. Additionally, the same behavior was observed in the F0.5 + N1.5 hybrid formulation for the average values of the tenacity after natural weathering. The formulation with 2.0% CNFs obtained superior average value of tenacity compared to the other formulations, after exposure to weather. The tenacity is associated to composite toughness, which is caused by several phenomena produced during composite fracture, such as debonding, pull-out, bridging, and fiber fracture [91]. CNF pull-out is probably the main factor responsible for the toughness mechanism and energy absorption by the cementitious composite [26]. The characteristics of the fracture surfaces provide a better understanding of the mechanical results. These results show that the CNFs exhibit good energy absorption when subjected to a load or tension, which can be due to a greater surface area when compared to fibers. Greater values of tenacity indicate that CNFs contribute more effectively to delay the start of crack propagation [49].

For the 0.5N formulation, there was a reduction in all mechanical properties after five months of natural

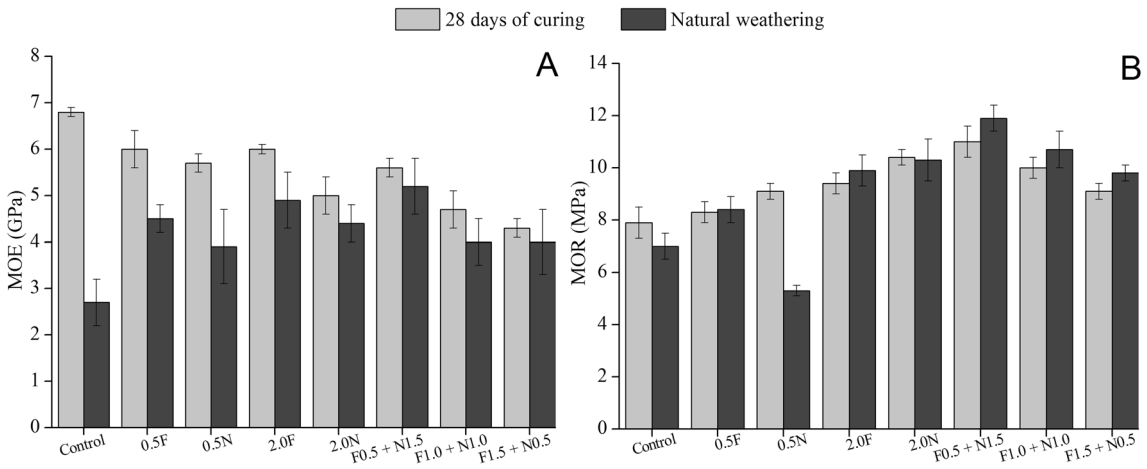

Fig. 10 Mechanical properties of the cementitious composites at 28 days of cure and after 5 months of natural weathering: **a** MOE; **b** MOR; 0.5F = 0.5% of fiber; 2.0F = 2.0% of fiber; 0.5 N = 0.5% of CNFs; 2.0 N = 2.0% of CNFs

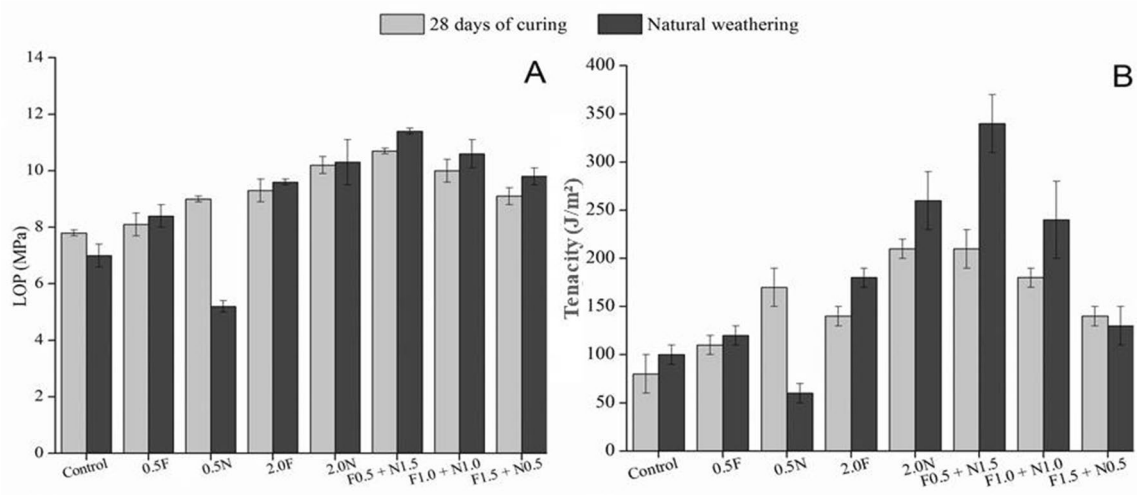

Fig. 11 Mechanical properties of the cementitious composites at 28 days of cure and after 5 months of natural weathering: **a** limit of proportionality (LOP) and **b** tenacity; 0.5F = 0.5% fiber; 2.0F = 2.0% fiber; 0.5 N = 0.5% CNFs; 2.0 N = 2.0% CNFs

weathering compared to the values presented after 28 days of curing. Some explanations can be given for the failure of this amount of reinforcement: (1) the low content of CNFs used as reinforcement may have accumulated in the stress zones, which may have compromised mechanical properties; (2) the non-uniform distribution of micro/nanofibrils in the matrix could lead to clumping, resulting in improper dispersion during mixing in the extruder screw; and (3) the low content of CNFs could have caused their mineralization when soaked in a high amount of cement matrix. After 28 days of curing and natural weathering, the hybrid formulations showed a trend of reducing the MOR proportionally to the quantity of CNFs. It was observed that after natural weathering, there was an increase in the MOR, LOP, and tenacity of the fiber–cement composites. These results indicate that the adhesion between the reinforcement and the matrix improved after natural weathering, which may be due to the reprecipitation of cement hydration products inside and around the fibers and CNFs and the consequent filling of the pores at the interface between the reinforcement and the matrix. The F0.5 + N1.5 formulations presented a predisposition to higher LOP values. Higher LOP values are evidence of an improved fiber-matrix adherence, which is a result of the higher surface area of CNFs that connect different grains and particles with different sizes, forming a network that delays plastic deformation in the cement matrix. Exposure of the composite to water during natural weathering provides the reintroduction of water into the system after the curing period. It also reactivates the dissolution of ions (mainly Ca^{2+}) from anhydrous grains and less stable cement phases, such as calcium hydroxide. These ions are generally transported and reprecipitated in the porous zones of the cementitious matrix, such as the interface between the fibers and the matrix [56]. The composites with the F0.5 + N1.5 hybrid formulation presented better mechanical properties than the other formulations, indicating greater mechanical performance and durability, especially on MOR and tenacity. The rupture of hydrogen bonds in the fiber-matrix interface allows the fibers pull-out, resulting in a composite with greater tenacity. If the physical bonds (from material packaging and densification) and the chemical bonds (hydrogen bonds) between the reinforcement and the matrix are very strong, the fiber does not slip, instead it breaks, resulting in a reduction in composite tenacity.

Conclusion

Fiber–cement composites were produced with the reinforcement of NaOH-treated jute fibers, CNFs, and hybrids of both, and their physical and mechanical properties were evaluated. NaOH treatment of raw jute fibers reduced the hemicelluloses content, thereby increasing the relative content of cellulose, as confirmed by the FTIR analysis. Alkaline treatment resulted in a slightly higher crystalline fraction and larger crystallite size of the treated fibers. TGA and DTG results showed higher thermal stability of the NaOH-treated jute fibers and CNFs when compared to raw fibers. Formulations exclusively with CNFs showed higher average apparent density values. The hybrid cement composites reinforced with 1.5% CNFs and 0.5% fibers showed stronger mechanical properties than the other formulations. The LOP for fiber–cement composites reinforced with 2% CNFs was approximately 24% higher than that of the control. The tenacity of the fiber–cement reinforced with CNFs exceeded that of the control and those reinforced with fibers.

The MOE values tended to decrease from the control to the reinforced composites, with the fiber reinforcement being superior to CNFs. The results showed that it is possible to improve the microstructure and mechanical performance of composites using small amounts of CNF reinforcement (0.5%–2%). CNFs acted as bridges for the stress transfer in the microstructure of the composites, decreasing the propagation of microcracks in the matrix. In general, natural weathering increased the MOR, LOP, and tenacity of the cement composites. The use of fiber and CNF hybrids as reinforcement allows the effects to be combined, thus resulting in improved mechanical properties when compared to fibers or CNFs used individually.

Acknowledgements The authors are grateful for the financial support provided by Conselho Nacional de Desenvolvimento Científico e Tecnológico (CNPq), Fundação de Amparo à Pesquisa do Estado de Minas Gerais (FAPEMIG), Coordenação de Aperfeiçoamento de Pessoal de Nível Superior (Capes) and Rede AgroNano (Embrapa), Rede BIOSMAT (FZEA/USP) e Rede RELIGAR (UFLA).

Author Contributions CSF conduction of work, MVS revision and discussions, LES experiments, as DRX, MAM experiments, as FTIR and microscopy images, MGJ revision of the text, GHT supervisor.

References

1. Fonseca, C.S., Silva, M.F., Mendes, R.F., Hein, P.R.G., Zangiacomo, A.L., Savastano, H., Tonoli, G.H.D.: Jute fibers and micro/nanofibrils as reinforcement in extruded fiber–cement composites. Constr. Build. Mater. **211**, 517–527 (2019). https://doi.org/10.1016/j.conbuildmat.2019.03.236
2. Sadiq, K.M., Bzeni, D.K.H., Shaikh, F.U.A.: Deflection hardening behaviour of jute strands reinforced lightweight cementitious composite. Constr. Build. Mater. **96**, 102–111 (2015). https://doi.org/10.1016/j.conbuildmat.2015.08.004
3. Jahan, M.S., Mostafizur Rahman, J.N.M., Islam, M., Quaiyyum, M.A.: Chemical characteristics of ribbon retted jute and its effect on pulping and papermaking properties. Ind. Crop. Prod. **84**, 116–120 (2016). https://doi.org/10.1016/j.indcrop.2016.01.054
4. Neto, J.R.A., Carvalho, L.H., Araújo, E.M.: Influence of a nanoparticulate filler addition on the mechanical properties of polyurethane/jute fiber composites. Polím. Cienc. Tecnol. **17**, 10–15 (2007). https://doi.org/10.1590/S0104-14282007000100006
5. Sanjay, M.R., Yogesha, B.: Studies on mechanical properties of jute/e-glass fiber reinforced epoxy hybrid composites. J. Miner. Mater. Charact. Eng. **4**, 15–25 (2007). https://doi.org/10.4236/jmmce.2016.41002
6. Rafiquzzaman, Maksundul, I., Habibur, R., Saniat, T., Nahid, H.: Mechanical property evaluation of glass–jute fiber reinforced polymer composites. Polym. Adv. Technol. **27**, 1308–1316 (2016). https://doi.org/10.1002/pat.3798
7. Ferreira, J.M., Capela, C., Manaia, J., Costa, J.D.: Mechanical properties of woven mat jute/epoxy composites. Mater. Res. **19**, 702–710 (2016). https://doi.org/10.1590/1980-5373-MR-2015-0422
8. Chakraborty, S., Kundu, S.P., Roy, A., Basak, R.K., Adhikari, B., Majumder, S.B.: Improvement of the mechanical properties of jute fibre reinforced cement mortar: a statistical approach. Constr. Build. Mater. **38**, 776–784 (2013). https://doi.org/10.1016/j.conbuildmat.2012.09.067
9. Jo, B., Chakraborty, S., Yoon, K.W.: A hypothetical model based on effectiveness of combined alkali and polymer latex modified jute fibre in controlling the setting and hydration behaviour of cement. Constr. Build. Mater. **68**, 1–9 (2014). https://doi.org/10.1016/j.conbuildmat.2014.06.043
10. Anglès, M., Dufresne, A.: Plasticized starch/tunicin whiskers nanocomposites: mechanical behavior. Macromolecules **34**, 2921–2931 (2001). https://doi.org/10.1021/ma001555h
11. Assis, L.M., Zavareze, E.R., Hernández, C.P., Soares, L.A.S.: Characteristics of nanoparticles and their potential applications in foods. Braz. J. Food Technol. **15**, 99–109 (2012). https://doi.org/10.1590/S1981-67232012005000004
12. Mortazavi, S., Moghaddam, M.K.: An analysis of structure and properties of a natural cellulosic fiber (Leafiran). Fibers Polym. **11**, 877–882 (2010). https://doi.org/10.1007/s12221-010-0877-z
13. Stelte, W., Sanadi, A.R.: Preparation and characterization of cellulose nanofibers from two commercial hardwood and softwood pulps. Ind. Eng. Chem. Res. **48**, 11211–11219 (2009). https://doi.org/10.1021/ie9011672
14. Wang, B., Sain, M.: Dispersion of soybean stock-based nanofiber in a plastic matrix. Polym. Int. **56**, 538–546 (2007). https://doi.org/10.1021/bk-2006-0938.ch013
15. Ferrer, A., Filpponen, I., Rodríguez, A., Laine, J., Rojas, O.J.: Valorization of residual Empty Palm Fruit Bunch Fibers (EPFBF) by microfluidization: production of nanofibrillated cellulose and EPFBF nanopaper. Bioresour. Tech. **125**, 249–255 (2012). https://doi.org/10.1016/j.biortech.2012.08.108
16. Padal, K.T., Ramji, K., Prasad, V.V.S.: Mechanical properties of jute nanofibres reinforced composites. Glob. J. Res. Eng. **14**, 1–6 (2014)
17. Maaloul, N., Oulego, P., Rendueles, M., Ghorbal, A., Díaz, M.: Novel biosorbents from almond shells: characterization and adsorption properties modeling for Cu(II) ions from aqueous solutions. J. Environ. Chem. Eng. **5**(3), 2944–2954 (2017). https://doi.org/10.1016/j.jece.2017.05.037
18. Saurabh, C.K., Mustapha, A., Masri, M.M., Owolabi, A.F., Syakir, M.I., Dungani, R., Paridah, M.T., Jawaid, M., Khalil, H.P.S.A.: Isolation and characterization of cellulose nanofibers from *Gigantochloa scortechiniias* a reinforcement material. J. Nanomater. (2016). https://doi.org/10.1155/2016/4024527
19. Thomas, M.G., Abraham, E., Jyotishkumar, P., Pothan, L.A., Maria, H.J., Thoma, S.: Nanocelluloses from jute fibers and their nanocomposites with natural rubber: preparation and characterization. Int. J. Biol. Macromol. **81**, 768–777 (2015). https://doi.org/10.1016/j.ijbiomac.2015.08.053
20. Bufalino, L., de SenaNeto, A.R., Tonoli, G.H.D., Fonseca, A.S., Costa, T.G., Marconcini, J.M., Colodette, J.L., Labory, C.R.G., Mendes, L.M.: How the chemical nature of Brazilian hardwoods affects nanofibrillation of cellulose fibers and film optical quality. Cellulose **22**, 3657–3672 (2015). https://doi.org/10.1007/s10570-015-0771-3
21. do Prado, N.R.T., Raabe, J., Mirmehdi, S., Hugen, L.N., Lima, L.C., Ramos, A.L.S., Guimarães, M., Jr., Tonoli, G.H.D.: Strength improvement of hydroxypropyl methylcellulose/starch films using cellulose nanocrystals. CERNE **23**, 423–434 (2018). https://doi.org/10.1590/01047760201723042303
22. Siqueira, G., Bras, J., Dufresne, A.: Cellulose whiskers versus microfibrils: influence of the nature of the nanoparticle and its surface functionalization on the thermal and mechanical properties of nanocomposites. Biomacromolecules **10**, 425–432 (2009). https://doi.org/10.1021/bm801193d
23. Alila, S., Besbesa, I., Vilar, M.R., Mutje, P., Boufi, S.: Non-woody plants as raw materials for production of microfibrillated

cellulose (MFC): a comparative study. Ind. Crop. Prod. **41**, 250–259 (2013). https://doi.org/10.1016/j.indcrop.2012.04.028
24. Alwani, M.S., Khalil, H.P.S.A., Sulaiman, O., Islam, M.N., Dungani, R.: An approach to using agricultural waste fibres in biocomposites application: thermogravimetric analysis and activation energy study. Bioresources **9**, 218–230 (2014). https://doi.org/10.15376/biores.9.1.218-230
25. Sri Aprilia, N.A., Hossain, M.D., Mustapha, A., SitiSuhaily, S., Nik Norulaini, N.A., Peng, L.C., Mohd Omar, A.K., Abdul Khalil, H.P.S.: Optimizing the isolation of microfibrillated bamboo in high pressure enzymatic hydrolysis. Bioresources **10**, 5305–5316 (2015). https://doi.org/10.15376/biores.10.3.5305-5316
26. Fonseca, C.S., Silva, T.F., Silva, M.F., Oliveira, I.R.C., Mendes, R.F., Hein, P.R.G., Mendes, L.M., Tonoli, G.H.D.: Eucalyptus cellulose micro/nanofibers in extruded fibercement composites. CERNE **22**, 1–9 (2016). https://doi.org/10.1590/01047760201622012084
27. Veloso, M.C.R.A., Pires, M.R., Villela, L.S., Scatolino, M.V., Protásio, T.P., Mendes, L.M., Guimarães, J.B., Jr.: Potential destination of Brazilian cocoa agro-industrial wastes for production of materials with high added value. Waste Manag. **118**, 36–44 (2020). https://doi.org/10.1016/j.wasman.2020.08.019
28. Silva, D.W., Scatolino, M.V., do Prado, N.R.T., Mendes, R.F., Mendes, L.M.: Addition of different proportions of castor husk and pine wood in particleboards. Waste Biomass Valor. **9**, 139–145 (2018). https://doi.org/10.1007/s12649-016-9742-7
29. Scatolino, M.V., de Costa, A.O., Guimarães, J.B., Jr., de Protásio, T.P., Mendes, R.F., Mendes, L.M.: Eucalyptus wood and coffee parchment for particleboard production: physical and mechanical properties. Cienc. Agrotec. **41**, 139–146 (2017). https://doi.org/10.1590/1413-70542017412038616
30. de Protásio, T.P., Mendes, R.F., Scatolino, M.V., Mendes, L.M., Trugilho, P.F., de Melo, I.C.N.A.: Thermal stability of particleboards of sugar cane bagasse and *Pinus* spp. wood. Sci. For. **43**, 683–691 (2015)
31. Lisboa, F.J.N., Scatolino, M.V., de Paula Protásio, T., et al.: Lignocellulosic materials for production of cement composites: valorization of the alkali treated soybean pod and eucalyptus wood particles to obtain higher value-added products. Waste Biomass Valor. **11**, 2235–2245 (2020). https://doi.org/10.1007/s12649-018-0488-2
32. Pereira, T.G.T., Silva, D.W., Eugênio, T.M.C., Scatolino, M.V., Terra, I.C.C., Fonseca, C.S., Bufalino, L., Mendes, R.F., Mendes, L.M.: Coconut fibers and quartzite wastes for fiber–cement production by extrusion. Mater. Today Proc. (2020). https://doi.org/10.1016/j.matpr.2020.01.394
33. Silva, D.W., Scatolino, M.V., Pereira, T.G.T., Vilela, A.P., Eugênio, T.M.C., Martins, M.A., Mendes, R.F., Bufalino, L., Tonoli, G.H.D., Mendes, L.M.: Influence of thermal treatment of eucalyptus fibers on the physical-mechanical properties of extruded fiber–cement composites. Mater. Today Proc. (2020). https://doi.org/10.1016/j.matpr.2020.04.764
34. Tonoli, G.H.D., Belgacem, M.N., Siqueira, G., Bras, J., Savastano, H., Rocco Lahr, F.A.: Processing and dimensional changes of cement based composites reinforced with surface-treated cellulose fibres. Cem. Concr. Compos. **37**, 68–75 (2013). https://doi.org/10.1016/j.cemconcomp.2012.12.004
35. Tonoli, G.H.D., Belgacem, M.N., Bras, J., Pereira-da-Silva, M.A., Rocco Lahr, F.A., Savastano, H.: Impact of bleaching pine fibre on the fibre/cement interface. J. Mater. Sci. **47**(9), 4167–4177 (2012). https://doi.org/10.1007/s10853-012-6271-z
36. Oancea, I., Bujoreanu, C., Budescu, M., Benchea, M., Grădinaru, C.M.: Considerations on sound absorption coefficient of sustainable concrete with different waste replacements. J. Clean. Prod. **203**, 301–312 (2018). https://doi.org/10.1016/j.jclepro.2018.08.273
37. Lahouioui, M., Ben Arfi, R., Fois, M., Ibos, L., Ghorbal, A.: Mechanical and acoustical properties of date palm fiber-reinforced cementitious composites. Waste Biomass Valor. (2019). https://doi.org/10.1007/s12649-019-00745-3
38. Sudin, R., Swamy, N.: Bamboo and wood fibre cement composites for sustainable infrastructure regeneration. J. Mater. Sci. **41**, 6917–6924 (2006). https://doi.org/10.1007/s10853-006-0224-3
39. Nakagaito, A.N., Yano, H.: Novel high-strength biocomposites based on microfibrillated cellulose having nanoorder-unit web-like network structure. Appl. Phys. A **80**, 155–159 (2005). https://doi.org/10.1007/s00339-003-2225-2
40. Yue, Y., Han, J., Han, G., Zhang, Q., Frenche, A.D., Wua, Q.: Characterization of cellulose I/II hybrid fibers isolated from energycane bagasse during the delignification process: morphology, crystallinity and percentage estimation. Carbohydr. Polym. **133**, 438–447 (2015). https://doi.org/10.1016/j.carbpol.2015.07.058
41. Brazilian Association of Technical Standards - ABNT NBR 14853: determination of soluble matter in ethanol-toluene and in dichloromethane and in acetone. NBR. (2010)
42. Brazilian Association of Technical Standards - ABNT NBR 7989: pulp and wood—determination of acid-insoluble lignin. NBR. (2010)
43. Browning, B.L.: The chemistry of wood. Interscience, New York (1963)
44. Kennedy, F., Phillips, G.O., Willians, P.A.: Wood and cellulosics, industrial utilization, biotechnology, structure and properties. Ellis Horwood, Chichester (1987)
45. Brazilian Association of Technical Standards - ABNT NBR 13999: determination of residue (ash) after incineration at 525 °C. NBR. (2003)
46. Lora, E.E.S., et al.: Gasification and pyrolysis for converting biomass to electricity and biofuels Biocombustíveis. EditoraIntegrada, Rio de Janeiro (2012)
47. Scatolino, M.V., Fonseca, C.S., Gomes, M.S., Rompa, V.D., Martins, M.A., Tonoli, G.H.D., Mendes, L.M.: How the surface wettability and modulus of elasticity of the Amazonian paricá nanofibrils films are affected by the chemical changes of the natural fibers. Eur. J. Wood Wood Prod. **76**, 1581–1594 (2018). https://doi.org/10.1007/s00107-018-1343-7
48. French, A.D.: Idealized powder diffraction patterns for cellulose polymorphs. Cellulose **21**, 885–896 (2014). https://doi.org/10.1007/s10570-013-0030-4
49. da Correia, V.C., dos Santos, V., Sain, M., Santos, S.F., Leão, A.L., Savastano, H., Jr.: Grinding process for the production of nanofibrillated cellulose based on unbleached and bleached bamboo organosolv pulp. Cellulose **23**, 2971–2987 (2016). https://doi.org/10.1007/s10570-016-0996-9
50. Nam, S., French, A.D., Condon, B.D., Concha, M.: Segal crystallinity index revisited by the simulation of X-ray diffraction patterns of cotton cellulose Ib and cellulose. Carbohyd. Polym. **135**, 1–9 (2016). https://doi.org/10.1016/j.carbpol.2015.08.035
51. Langford, J.I., Wilson, A.J.C.: Scherrer after sixty years: a survey and some new results in the determination of crystallite size. J. Appl. Crystallogr. **11**, 102–113 (1978). https://doi.org/10.1107/S0021889878012844
52. Ballesteros, J.E.M., dos Santos, V., Mármol, G., Frías, M., Fiorelli, J.: Potential of the hornification treatment on eucalyptus and pine fibers for fiber–cement applications. Cellulose **24**, 2275–2286 (2017). https://doi.org/10.1007/s10570-017-1253-6
53. Teixeira, R.S., Tonoli, G.H.D., Santos, S.F., Fiorelli, J., Savastano Junior, H., Lahr, F.A.R.: Extruded cement based composites reinforced with sugar cane bagasse fibres. Key Eng. Mater. **517**, 450–457 (2017). https://doi.org/10.4028/www.scientific.net/KEM.517.450
54. American Society for Testing and Materials–ASTM C 948-81: Test method for dry and wet bulk density, water absorption, and

apparent porosity of thin sections of glass-fiber reinforced concrete. West Conshohocken. 2 p (2001)
55. Rilem—Technical committee 49 TFR: testing methods for fibre reinforced cement-based composites. Mater. Struct 17:441-456. (1984)
56. Tonoli, G.H.D., Santos, S.F., Joaquim, A.P., Savastano, H., Jr.: Effect of accelerated carbonation on cementitious roofing tiles reinforced with lignocellulosic fibre. Constr. Build. Mater. **24**, 193–201 (2010). https://doi.org/10.1016/j.conbuildmat.2007.11.018
57. Tonoli, G.H.D., Santos, S.F., Savastano, H., Jr., Delvasto, S., Mejía de Gutiérrez, R., del Lopez de Murphy, M.M.: Effects of natural weathering on microstructure and mineral composition of cementitious roofing tiles reinforced with fique fibre. Cem. Concr. Res. **33**, 225–232 (2011). https://doi.org/10.1016/j.cemconcomp.2010.10.013
58. Fonseca, A.S., Mori, F.A., Tonoli, G.H.D., Savastano, H., Jr., Ferrari, D.L., Miranda, I.P.A.: Properties of an Amazonian vegetable fiber as a potential reinforcing material. Ind. Crop. Prod. **47**, 43–50 (2013). https://doi.org/10.1016/j.indcrop.2013.02.033
59. Iwamoto, S., Abe, K., Yano, H.: The effect of hemicelluloses on wood pulp nanofibrillation and nanofiber network characteristics. Biomacromolecules **9**, 1022–1026 (2008). https://doi.org/10.1021/bm701157n
60. Marques, G., Rencoret, J., Gutiérrez, A., Del Río, J.C.: Evaluation of the chemical composition of different non-woody plant fibres used for pulp and paper manufacturing. Open Agric. J. **4**, 93–101 (2010). https://doi.org/10.2174/1874331501004010093
61. Spence, K.L., Venditti, R.A., Rojas, O.J., Habibi, Y., Pawlak, J.J.: The effect of chemical composition on microfibrillar cellulose films from wood pulps: water interactions and physical properties for packaging applications. Cellulose **17**, 835–848 (2010). https://doi.org/10.1007/s10570-010-9424-8
62. Chaker, A., Alila, S., Mutjé, P., Vilar, M.R., Boufi, S.: Key role of the hemicellulose content and the cell morphology on the nanofibrillation effectiveness of cellulose pulps. Cellulose **20**, 2863–2875 (2013). https://doi.org/10.1007/s10570-013-0036-y
63. Dias, M.C., Mendonça, M.C., Damásio, R.A.P., Zidanes, U.L., Mori, F.A., Ferreira, S.R., Tonoli, G.H.D.: Influence of hemicellulose content of eucalyptus and *Pinus* fibers on the grinding process for obtaining cellulose micro/nanofibrils. Holzforschung **73**, 1035–1046 (2019). https://doi.org/10.1515/hf-2018-0230
64. SenaNeto, A.R., Araujo, M.A.M., Souza, F.V.D., Mattoso, L.H.C., Marconcini, J.M.: Characterization and comparative evaluation of thermal, structural, chemical, mechanical and morphological properties of six pineapple leaf fiber varieties for use in composites. Ind. Crop. Prod. **43**, 529–537 (2013). https://doi.org/10.1016/j.indcrop.2012.08.001
65. de Paula Protásio, T., Scatolino, M.V., de Araújo, A.C.C., et al.: Assessing proximate composition, extractive concentration, and lignin quality to determine appropriate parameters for selection of superior eucalyptus firewood. Bioenerg. Res. **12**, 626–641 (2019). https://doi.org/10.1007/s12155-019-10004-x
66. López-Gonzales, D., Fernandez-Lopez, M., Valverde, J.L., Sanchez-Silva, L.: Thermogravimetric mass spectrometric analysis. Bioresour. Technol. **143**, 562–574 (2013)
67. Tonoli, G.H.D., Holtman, K.M., Glenn, G., Fonseca, A.S., Wood, D., Williams, T., Sa, V.A., Torres, L., Klamczynski, A., Orts, W.J.: Properties of cellulose micro/nanofibers obtained from eucalyptus pulp fiber treated with anaerobic digestate and high shear mixing. Cellulose **23**, 1239–1256 (2016). https://doi.org/10.1007/s10570-016-0890-5
68. Nishiyama, Y., Langan, P., Chanzy, H.: Crystal structure and hydrogen bonding system in cellulose Iα from synchrotron X-ray and neutron fiber diffraction. J. Am. Chem. Soc. **125**, 14300–14306 (2003). https://doi.org/10.1021/ja0257319
69. Correa, A.C., Teixeira, E.M., Pessan, L.A., Matoso, L.H.C.: Cellulose nanofibers from curaua fibers. Cellulose **17**, 1183–1192 (2010). https://doi.org/10.1007/s10570-010-9453-3
70. Ass, B.A.P., Belgacem, M.N., Frollini, E.: Mercerized linters cellulose: characterization and acetylation in N,N-dimethylacetamide/lithium chloride. Carbohyd. Polym. **63**, 19–29 (2006). https://doi.org/10.1016/j.carbpol.2005.06.010
71. Benziman, M., Haigler, C.H., Brown, R.M., Jr., White, A.R., Cooper, K.M.: Cellulose biogenesis: polymerization and crystallization are coupled processes in *Acetobacter xylinum*. Proc. Natl Acad. Sci. USA **77**, 6678–6682 (1980). https://doi.org/10.1073/pnas.77.11.6678
72. Rosa, M.F., Medeiros, E.S., Malmonge, J.A., Gregorski, K.S., Wood, D.F., Mattoso, L.H.C., Glenn, G., Orts, W.J., Imam, S.H.: Cellulose nanowhiskers from coconut husk fibers: effect of preparation conditions on their thermal and morphological behavior. Carbohyd. Polym. **81**, 83–92 (2010). https://doi.org/10.1016/j.carbpol.2010.01.059
73. Tischer, P.C.S.F., Sierakowski, M.R., Westfahl, H., Jr., Tischer, C.A.: Nanostructural reorganization of bacterial celulose by ultrasonic treatment. Biomacromolecules **11**, 1217–1224 (2010). https://doi.org/10.1021/bm901383a
74. Scatolino, M.V., Bufalino, L., Mendes, L.M., Guimarães, M., Jr., Tonoli, G.H.D.: Impact of nanofibrillation degree of eucalyptus and Amazonian hardwood sawdust on physical properties of cellulose nanofibril films. Wood Sci. Technol. **51**, 1–21 (2017). https://doi.org/10.1007/s00226-017-0927-4
75. Alemdar, A., Sain, M.: Isolation and characterization of nanofibers from agricultural residues: wheat straw and soy hulls. Bioresour. Technol. **99**, 1664–1671 (2008). https://doi.org/10.1016/j.biortech.2007.04.029
76. Siró, I., Plackett, D.: Microfibrillated cellulose and new nanocomposite materials: a review. Cellulose **17**, 459–494 (2010). https://doi.org/10.1007/s10570-010-9405-y
77. Syverud, K., Chinga Carrasco, G., Toledo, J., Toledo, P.G.: A comparative study of eucalyptus and *Pinus radiata* pulp fibres as raw materials for production of cellulose nanofibrils. Carbohyd. Polym. **17**, 1033–1038 (2011). https://doi.org/10.1016/j.carbpol.2010.12.066
78. Lin, J., Yu, L., Tian, F., Zhao, N., Li, X., Bian, F., Wang, J.: Cellulose nanofibrils aerogels generated from jute fibers. Carbohyd. Polym. **109**, 35–43 (2014). https://doi.org/10.1016/j.carbpol.2014.03.045
79. Das, K., Ray, D., Banerjee, C., Bandyopadhyay, N.R., Sahoo, S., Mohanty, A.K., Misra, M.: Physicomechanical and thermal properties of jute-nanofiber-reinforced biocopolyester composites. Ind. Eng. Chem. Res. **49**, 2775–2782 (2010). https://doi.org/10.1021/ie9019984
80. Almeida, A.E.F.S., Tonoli, G.H.D., Santos, S.F., Savastano, H., Jr.: Improved durability of vegetable fiber reinforced cement composite subject to accelerated carbonation at early age. Cem. Conc. Comp. **42**, 49–58 (2013). https://doi.org/10.1016/j.cemconcomp.2013.05.001
81. Pizzol, V.D., Mendes, L.M., Frezzatti, L., Savastano, H., Jr., Tonoli, G.H.D.: Effect of accelerated carbonation on the microstructure and physical properties of hybrid fiber–cement composites. Miner. Eng. **59**, 101–106 (2014). https://doi.org/10.1016/j.mineng.2013.11.007
82. Tonoli, G.H.D., Rodrigues Filho, U.P., Savastano, H., Jr., Bras, J., Belgacem, M.N., Rocco Lahr, F.A.: Cellulose modified fibres in cement based composites. Composites A **40**, 2046–2053 (2009). https://doi.org/10.1016/j.compositesa.2009.09.016
83. Mohr, B.J., Biernacki, J.J., Kurtis, K.E.: Supplementary cementitious materials for mitigating degradation of kraft pulp fiber–cement composites. Cem. Concr. Res. **37**, 1531–1543 (2007). https://doi.org/10.1016/j.cemconres.2007.08.001

84. Hover, K.: The influence of water on the performance of concret. Constr. Build. Mater. **25**, 3003–3013 (2011). https://doi.org/10.1016/j.conbuildmat.2011.01.010
85. Peschard, A., Govin, A., Pourchez, J., Fredon, E., Bertrand, L., Maximilien, S., Guilhot, B.: Effect of polysaccharides on the hydration of cement suspension. J. Eur. Ceram. Soc. **26**, 1439–1445 (2006). https://doi.org/10.1016/j.jeurceramsoc.2005.02.005
86. Campilho, R.D.S.G.: Natural fiber composites, 1st edn. CRC Press, Boca Raton (2015)
87. Vaxman, A., Narkis, M., Siegmann, A., Kenig, S.: Void formation in short-fiber thermoplastic composites. Polym. Compos. **10**, 449–453 (1989). https://doi.org/10.1002/pc.750100609
88. Wang, J., Xu, H., Xu, D., Du, P., Zhou, Z., Yuan, L., Cheng, X.: Accelerated carbonation of hardened cement pastes: influence of porosity. Const. Build. Mater. **225**, 159–169 (2019). https://doi.org/10.1016/j.conbuildmat.2019.07.088
89. Liu, R., Xiao, H., Li, H., Sun, L., Pi, Z., Waqar, G.Q., Du, T., Yu, L.: Effects of nano-SiO_2 on the permeability-related properties of cement-based composites with different water/cement ratios. J. Mater. Sci. **53**, 4974–4986 (2018). https://doi.org/10.1007/s10853-017-1906-8
90. Teixeira RS.: Effect of curauá and polypropylene fibers on the performance of cementitious composites produced by extrusion. p 149 Thesis (PhD in Materials Science and Engineering)—University of São Paulo, São Carlos. Brazil (2015)
91. Almeida, A.E.F.S., Tonoli, G.H.D., Santos, S.F., Savastano, H., Jr.: Accelerated carbonation in the early ages of cellulose pulps reinforced cement composites. Ambient. Constr. **10**, 233–246 (2010). https://doi.org/10.1590/S1678-86212010000400016